Neural stem cell-mediated CE/CPT-11 enzyme/prodrug therapy in transgenic mouse model of intracerebellar medulloblastoma

Margarita Gutova[1,*], **Gregory M. Shackleford**[6], **Vazgen Khankaldyyan**[5], **Kelsey A. Herrmann**[1], **Xiang-He Shi**[6,8], **Kimberly Mittelholtz**[6], **Yelena Abramyants**[1], **M. Suzette Blanchard**[2], **Seung U. Kim**[7], **Alexander J. Annala**[1], **Joseph Najbauer**[1], **Timothy W. Synold**[4], **Massimo D'Apuzzo**[3], **Michael E. Barish**[1], **Rex A. Moats**[5,*,†], and **Karen S. Aboody**[1,†]

[1]Department of Neurosciences, Beckman Research Institute of the City of Hope, Duarte, CA 91010

[2]Division of Information Sciences, Beckman Research Institute of the City of Hope, Duarte, CA 91010

[3]Department of Pathology, Beckman Research Institute of the City of Hope, Duarte, CA 91010

[4]Division of Clinical and Molecular Pharmacology, Beckman Research Institute of the City of Hope, Duarte, CA 91010

[5]Department of Radiology, USC Keck School of Medicine and The Saban Research Institute of Children's Hospital Los Angeles, Los Angeles, CA 90027

[6]Division of Hematology-Oncology, USC Keck School of Medicine and The Saban Research Institute of Children's Hospital Los Angeles, Los Angeles, CA 90027

[7]Division of Neurology, Department of Medicine, UBC Hospital, University of British Columbia, Vancouver, BC, Canada

[8]Medical Research Institute, Chung-Ang University College of Medicine, Seoul, Korea

Abstract

Medulloblastoma is a heterogeneous diffuse neoplasm that can be highly disseminated, and is the most common malignant childhood brain tumor. Although multimodal treatments have improved survival rates for patients with medulloblastoma, these tumors are associated with high morbidity and mortality. New treatment strategies are urgently needed to improve cure rates and, importantly, to spare normal brain tissue from neurotoxicity and patients from life-long cognitive and functional deficits associated with current therapies. In numerous preclinical brain tumor

---

*Correspondence: Margarita Gutova, M.D. Assistant Research Professor, Department of Neurosciences, Beckman Research Institute of the City of Hope, 1500 E. Duarte Road, Duarte, CA 91010-3000, Tel: (626) 359-8111 x65637, mgutova@coh.org; Rex A. Moats, Ph.D. Assistant Professor Department of Radiology, Pathology and Biomedical Engineering, Keck School of Medicine, University of Southern California, Director of Small Animal Imaging Research Center, The Saban Research Institute, Children's Hospital of Los Angeles, Tel: 406-650-7120, RMoats@chla.usc.edu.

†The laboratories of KS Aboody and RA Moats contributed equally to this work as part of a City of Hope – Children's Hospital of Los Angeles research collaboration

Conflict of interest: The authors state no conflict of interest.

models, neural stem cells (NSCs) have shown great promise as delivery vehicles for therapeutic genes. Here, we have used an established, genetically modified human NSC line (HB1.F3.CD) to deliver carboxylesterase (CE) to cerebellar tumor foci and locally activate the prodrug CPT-11 (Irinotecan) to the potent topoisomerase I inhibitor SN-38. HB1.F3.CD NSC tumor tropism, intratumoral distribution and therapeutic efficacy were investigated in clinically relevant experimental models. Magnetic resonance imaging was used for *in vivo* tracking of iron nanoparticle-labeled NSCs, and to assess the therapeutic efficacy of CE-expressing HB1.F3.CD cells. As compared to controls, a significant decrease in tumor growth rate was seen in mice that received both NSCs and CPT-11 as their treatment regimen. Thus, this study provides proof-of-concept for NSC-mediated CE/CPT-11 treatment of medulloblastoma, and serves as a foundation for further studies toward potential clinical application.

Keywords

carboxylesterase; CPT-11; gene therapy; irinotecan; MRI; medulloblastoma; neural stem cells; pediatric cancer; mouse model

Introduction

Primary brain cancer is the second most common cancer during childhood and the leading cause of cancer-related death in children ages 1-15 years.[1] Medulloblastoma is one of the most common of these diffuse and highly disseminated brain tumors, with a mean age of onset within the first 6 years of life.[2] Although the majority of patients with medulloblastoma can be treated with multimodality therapy, craniospinal radiation can have devastating effects on neurocognitive development and skeletal growth, and also poses a risk of initiating secondary tumors. Additional major obstacles to successful treatment of pediatric brain tumors include the blood-brain barrier, which prevents many anti-cancer agents from entering the brain, and therapeutic dose limitations due to toxicity to normal tissues. Although advances in surgical resection, refinements in radiation delivery and the addition of chemotherapy have improved survival rates for patients with medulloblastoma, it is still fatal in approximately one third of patients.[3] Those children who survive are often affected by delayed consequences of radiation and chemotherapy, which include permanent neurocognitive impairment, psychosocial deficits, stunted growth and endocrine deficiencies.[3-5] To significantly improve clinical outcome, both in terms of survival and quality of life of these patients, novel treatment strategies must be developed that specifically target tumor cells while sparing neurons in order to maintain normal brain development and function.

Neural stem cells (NSCs), by virtue of their inherent tumor-tropic properties, offer an unprecedented advantage of therapeutic specificity over conventional cancer treatments.[6-8] Because NSCs can effectively cross the blood-brain barrier and selectively target anti-cancer agents to invasive tumor cells, local drug concentrations and the therapeutic index can be increased while minimizing toxicity to normal tissues.[9] It is especially important for pediatric patients that neurons, oligondendrocytes and endogenous NSCs are spared, in order to preserve cognitive function and normal brain development. In the studies presented here,

we modified an established human NSC line (HB1.F3.CD) currently in Phase I clinical trial for treatment of recurrent glioblastoma in adults to deliver rabbit carboxylesterase (rCE) to enzymatically convert the prodrug CPT-11 (Irinotecan) to the potent topoisomerase inhibitor SN-38.[10-12] This NSC-mediated enzyme/prodrug therapy has demonstrated significant therapeutic efficacy in a metastatic human neuroblastoma model in mice.[11,12] In the current experiments, we labeled the rCE-secreting NSCs (HB1.F3.CD.rCE) with iron nanoparticles to allow for visualization and tracking of their tumor tropism by magnetic resonance imaging (MRI).[13-15] Biodistribution and therapeutic efficacy studies of NSC-mediated rCE/CPT-11 therapy were performed in immunocompetent transgenic and immunodeficient intracerebellar mouse models of medulloblastoma. High-power images of serial histopathological brain tissue sections revealed that NSCs were distributed within the tumor and adjacent to infiltrating tumor cells. MRI measurements of tumor volumes showed that mice treated with HB1.F3.CD.rCE NSCs, followed by intravenous (i.v.) administration of CPT-11, showed a significant decrease in tumor growth rate and volume when compared to mice treated with CPT-11 alone. Taken together, these studies provide proof-of-concept for NSC-mediated CE/CPT-11 treatment of medulloblastoma, and serve as a foundation for further studies toward potential clinical application.

Results

NSC migration and tumor cell killing assays in vitro

To investigate the directed migration of HB1.F3.CD NSCs to medulloblastoma cells *in vitro*, we performed Boyden chamber cell migration assays. Conditioned media (CM) derived from transgenic mouse medulloblastoma (cell lines 144-4, 108-2, 157-7) and human medulloblastoma (Daoy, UW228) cells were used as chemoattractants for NSCs. HB1.F3.CD cells demonstrated robust migration to tumor-conditioned media from all murine and human medulloblastoma cells, with the greatest migration to human Daoy and UW228 (primary human medulloblastoma) cells,[16] when compared to positive (10% FBS) and negative (2% BSA) controls (Figure 1a). HB1.F3.CD cells were labeled with iron nanoparticles (Ferumoxide and Protamine sulfate, FE-Pro), as previously described.[15,17] Neither labeling of cells with iron nor adenovirally transducing them with the rCE gene significantly affected their *in vitro* migration (Figure S1).

To determine CPT-11 and SN-38-mediated growth inhibition and cell killing of medulloblastoma cells, we generated mouse medulloblastoma cell cultures from dissociation of transgenic tumors (144-4) or used established human medulloblastoma cell lines (Daoy and UW228). Cells were incubated for 72 h in culture media containing various concentrations of CPT-11 (0-100 μM) or SN-38 (0-100 nM) alone, or CPT-11 (0-100 μM) in the presence of NSC-secreted rCE in the culture media. After incubation, the numbers of viable cells were determined by WST-1 or Guava ViaCount assay, and drug toxicity was calculated compared to zero drug controls. SN-38 was approximately 1,000-fold more potent than CPT-11; medulloblastoma cells had an IC_{50} for CPT-11 in the concentration range of 0.18 – 17.5 μM, while that for SN-38 was 0.2-2.2 nM (Figure 1b, c). The IC_{50} values for Daoy cells were 41 μM and 25.9 nM for CPT-11 and SN-38, respectively (data not shown). Conditioned media from rCE-secreting HB1.F3.CD cells (rCE enzyme activity

at 341 units/min) were used in combination with CPT-11 to sensitize human UW228 cells to the CPT-11 prodrug (Figure 1c). The IC_{50} for CPT-11 for UW228 cells was 17.5 μM and that for SN-38 was 2.2 nM. However, in the presence of rCE, the IC_{50} for CPT-11 was decreased by approximately 300-fold to 53 nM. The rCE expressed by the NSCs sensitized the target tumor cells to CPT-11 by producing SN-38 in the culture media (Figure S2). The *in vitro* kinetics of the CPT-11 to SN-38 conversion catalyzed by rCE was confirmed by LC-MS/MS analysis (Figure S2).

In vivo migration of iron-labeled HB1.F3.CD.rCE NSCs to medulloblastoma

To determine the tumor tropism and intratumoral distribution of HB1.F3.CD.rCE NSCs *in vivo*, two mouse models of medulloblastoma were used: 1) an immunocompetent transgenic model that mimics the tumor histopathology of human patients (Figure 2a), (Shackleford et al., manuscript in preparation), and 2) an intracerebellar human medulloblastoma (Daoy) xenograft model in *nude/nude* mice (Figure 2b).[7] In the transgenic model, medulloblastomas were induced in the developing cerebellum of mice by activating the Sonic Hedgehog (Shh) and Mycn pathways in granule neuron progenitor cells of the external granular layer that were targeted using an avian retrovirus, and tumor growth was monitored by firefly luciferase luminescence and MRI. Advantages of the transgenic medulloblastoma model include: 1) endogenous emergence of tumors by activation of signaling pathways involved in human disease in the presumed cell-of-origin, and 2) non-invasive real-time monitoring of tumor development by bioluminescence imaging or MRI. Among the advantages of the orthotopic human medulloblastoma model is the ability to evaluate biodistribution of NSCs in a human tumor xenograft model *in vivo*.

FE-Pro-labeled HB1.F3.CD.rCE NSCs were administered by intracerebellar (i.c.) injection (1×10^5 cells/2 μl PBS) into mice with detectable transgenic medulloblastoma tumors and human Daoy xenografts (Figure 3). NSCs injected i.c. ipsilateral to transgenic and Daoy tumors migrated and distributed into the tumor parenchyma and invasive tumor areas (Figure 3c, d, h, i). The NSC migration was monitored by MRI on days 1 and 4 after injection (Figure 3a, f). The hypointense MRI signal around the tumor likely reflects NSCs that are in the process of migration from the NSC injection site to tumors, but may not have reached their tumor target yet or have accumulated in the vicinity of tumor.

Brain tissue was harvested at day 6 post-NSC administration and histological sections were processed for Prussian blue staining to visualize iron-labeled NSCs. NSCs were detected as single cells or groups of NSCs within the tumor, as well as at the tumor periphery (Figure 3b, c, d, g, h, i). Figure 3, panels c and h, show Prussian blue-labeled NSCs deep in the tumor or close to the tumor edge (within 150 μm of the tumor edge). The Prussian blue-labeled NSCs in Figure 3i (lower right arrow) indicate the NSC injection site. NSCs were not detected in normal-appearing regions of the cerebellum or forebrain. These data suggest tumor-directed distribution of NSCs.

Both human and mouse tumors stained for the proliferation marker Ki-67 displayed areas of high proliferative activity as compared to islands of more differentiated tumor cells, a histopathological hallmark of medulloblastoma in human patients (Figure 3e, j). When NSCs were injected i.v. (1×10^6 cells/100 μl PBS), we observed homing of these cells to the

tumor in a similar patchy distribution, with extravasated NSCs often found along blood vessels or in perivascular spaces (Figure S3).

NSC-mediated rCE/CPT-11 therapeutic efficacy in medulloblastoma-bearing mice

We then evaluated the *in vivo* efficacy of NSC-mediated enzyme/prodrug (rCE/CPT-11) therapy in the transgenic murine medulloblastoma model. Transgenic mice that received Shh and Mycn gene-carrying viruses on postnatal day (PND) 3 were MR imaged every 2 weeks for tumor detection. Approximately 1.5 months after virus injection (PND 50), mice that developed tumors detectable by MRI were selected for NSC and CPT-11 treatment (mice that developed hydrocephalus were excluded from the study). A total of 14 mice were divided into four groups. Two treatment groups of four mice each received an intracerebellar injection of HB1.F3.CD.rCE cells (1×10^5 cells), followed by CPT-11 four days later. The two i.v. CPT-11 treatment regimens used reflect clinical dosing schedules: T1) a single high-dose injection of CPT-11 (38 mg/kg), or T2) multiple low-dose injections of CPT-11 (20 mg/kg/day $\times$ 4 days). One week later, each treatment group received a second round of NSCs plus CPT-11. Each experimental group was paired with a CPT-11 only control group of three mice each that were treated with the same CPT-11 regimens but without NSCs (C1 and C2, respectively).

Evaluation of tumor growth and treatment efficacy was performed by MRI beginning at 1 month (PND 30) and continuing thereafter (PND 50, 58, and 71). Tumor growth was inhibited in mice that received either therapeutic regimen T1 or T2 when compared to control groups C1 and C2. In addition, MRI revealed a reduction in tumor size and edema in the brains in treatment groups when compared to controls (Figure 4).

Statistical analysis of the kinetics of tumor growth was performed using linear mixed effects models. Comparisons of tumor growth rates between the treatment groups were done for pre-specified contrasts using *t*-tests. The average tumor growth rate between days 50 and 71 was 4.17 mm^3/day in the C1 control group, but was only 0.73 mm^3/day in the T1 treatment group (difference = -3.44, SE = 1.56, p = 0.04). The difference in tumor growth rates between the C2 control group (2.26 mm^3/day) and the T2 treatment group (-0.46 mm^3/day) was not significant (difference = -2.72, SE = 1.86, p = 0.16) and the difference in tumor growth rates between the T2 and T1 treatment groups was not significant (difference = -1.19, SE = 1.56, p = 0.45). The between mouse standard deviation for the tumor growth rates was 2.03 mm^3/day and the within mouse standard deviation was 2.88 mm^3. Figure 5b depicts the mean tumor growth rates and actual data points before and after treatment for each of the four groups. Figure 5c shows the tumor growth rates after treatment, as calculated using simple linear regression for each mouse and graphed by study group.

Therapeutic efficacy was also evaluated by histopathological analysis (hematoxylin and eosin staining) and 3D reconstruction of medulloblastoma tumors (mice were euthanized at PND 71) (Figure S4). These results corroborated the data obtained by MRI and showed that mice treated with intracerebellar injections of NSCs and CPT-11 had an overall smaller tumor volume when compared to mice treated with i.v. injection of CPT-11 alone on the same schedule of administration (Figure S4). Taken together, these results provide the first

evidence for a therapeutic effect of NSC-mediated rCE/CPT-11 enzyme prodrug therapy for orthotopic medulloblastoma in preclinical animal models.

Discussion

Advances in treatment of childhood medulloblastoma have dramatically improved the survival rates of standard-risk patients. However, overall therapeutic improvement has come with the cost of significant adverse effects among survivors, notably cognitive dysfunction.[18] Patients with high-risk medulloblastoma, metastatic disease or post-operative residual tumor, when treated with currently available treatments have relatively low 5-year event-free survival (25-40%).[1]

The efficacy of CPT-11 was previously investigated in a Phase II trial for children with high-risk malignant brain tumors, as well as in preclinical mouse models of medulloblastoma.[19,20] Limitations of current therapies include the low achievable CPT-11 concentration at the tumor site, and consequent high rate of tumor progression after initial treatment. Furthermore, CPT-11 therapy in children with brain tumors causes systemic toxicities such as myelosuppression and diarrhea.[19,21] Our study aims at development of an NSC-mediated enzyme/prodrug therapy to treat medulloblastoma which may help to overcome limitations of currently-available therapies. Our previous *in vitro* studies demonstrated that SN-38 is ∼1000-fold more effective at killing melanoma cells than is CPT-11 alone.[22]

When injected *in vivo*, NSCs can migrate long distances and target tumor areas, making them ideal for delivery of therapeutic genes, including prodrug-activating enzymes and antibodies.[23,24] NSC-mediated enzyme/prodrug therapy provides a strategy to circumvent the blood-brain barrier and overcome systemic toxicities by localized production of the active drug (SN-38) at the tumor site and providing a heretofore unachievable therapeutic specificity for malignant pediatric brain tumors.[6,7,25,26] Because NSCs home to hypoxic regions of brain tumors where cancer stem cells reside, they may aid in the eradication of this population of cancer cells as well.[27] It will also be important to investigate whether our NSC-mediated rCE/CPT-11 therapy can target the various subtypes of medulloblastoma and eliminate tumor-initiating cells.[28,29]

To our knowledge this is the first report to investigate NSC-mediated therapy in a transgenic mouse model of medulloblastoma. We also used an orthotopic human Daoy medulloblastoma xenograft model to evaluate NSC homing, biodistribution in the tumor, as well MRI-based *in vivo* monitoring of iron nanoparticle (Feridex)-labeled NSC migration. For the *in vivo* therapeutic study, we have chosen a new retrovirus-based Shh pathway-induced transgenic mouse model that closely replicates the conditions of spontaneous human medulloblastoma tumors (Shackleford et al., manuscript in preparation). Treatment of mice bearing murine medulloblastoma with NSC.rCE+CPT-11 resulted in reduction of the tumor growth rate and volume in these mice as compared to mice treated with CPT-11 alone.

The ability to monitor the *in vivo* migration and fate of therapeutic NSCs is an important aspect of stem cell-mediated gene therapy, Several studies have investigated the labeling of

stem cells with reporter genes or various contrast agents to enable non-invasive cell tracking, as well as quantification of the fate of the administered stem cells *in vivo*.[30] Although labeling of stem cells with fluorescent and bioluminescent reporter genes for visualization can be used in animal models, it cannot be used in humans. For this reason, we loaded NSCs with iron oxide nanoparticles prior to administration in order to track their migration and tumor distribution over time by MRI.[31] MRI is already the primary method of assessing therapeutic responses in brain tumor clinical trials.

In preclinical studies, our group has demonstrated the effective use of MRI to track iron-labeled NSCs, as well as the retention of NSC properties after iron labeling, including viability, tumor-tropism, transgene expression and lack of tumorigenicity and acute toxicity.[15] Other work has shown the utility of preclinical MRI for tracking iron-labeled leukocytes and mesenchymal stem cells (MSCs).[32] The safe use of iron oxide MRI contrast agents has been demonstrated in clinical research studies for central nervous system tumor visualization, and for diagnostic MRI purposes following intravenous administration.[33] Based on these reports, we believe the superparamagnetic iron oxide (SPIO) labeling technique may be safely and effectively used in the clinical setting to track NSCs introduced into the brain after tumor resection.

NSC-mediated gene therapies have been previously validated in preclinical models of neuroblastoma, melanoma brain metastases and glioma.[6,11,22,34] The current results provide preclinical proof-of-concept in support of NSC-mediated CE/CPT-11 enzyme/prodrug therapy for medulloblastoma, warranting further studies toward translation of this treatment strategy to clinical application. Of translational significance, the same NSC line used in these studies are currently being used in clinical Phase I trials in adult patients with recurrent high-grade glioma (clinical trial ID # NCT01172964; http://clinicaltrials.gov/ct2/show/NCT01172964). This trial is the first-in-human to use an immortalized, clonal, expandable NSC line, and the first to use NSCs to deliver a therapeutic agent for cancer treatment. We envision further modification of this GMP NSC Master Cell Bank to secrete CE, followed by injection directly into the cerebellum of medulloblastoma patients at the time of surgical resection or biopsy. Patients would then receive intravenous administration of CPT-11 to generate SN-38 locally at the tumor sites, to effect a significant anti-cancer response while minimizing toxicities to normal tissues. Although these NSCs are HLA Class II negative, patients would be placed on dexamethasone during each course of NSC and prodrug administration to minimize any potential immune response. Larger, longer term pre-clinical medulloblastoma studies are planned to optimize the CE/CPT-11 therapeutic regimen.

Materials and methods

Cell lines—Human Daoy medulloblastoma cells (ATCC, HTB-186) and UW228 human meduloblastoma cells (gift from Dr. Rolando F. Del Maestro, McGill University) were cultured in Dulbecco's Modified Eagle's Medium (DMEM) (Invitrogen, Carlsbad, CA) supplemented with 10% fetal bovine serum (FBS). Murine medulloblastoma cells were obtained at necropsy of tumor-bearing transgenic mice at Children's Hospital Los Angeles. To generate cell lines, cells were dissociated from murine tumors, and were cultured initially in Neurobasal medium with B27 (Invitrogen) and 20% FBS and later in DMEM

supplemented with 10% FBS. Human medulloblastoma Daoy xenografts were established in *nude/nude* mice (1×10^5 cells/2 μl). HB1.F3.CD NSCs were cultured (6% CO_2, 37°C) as an adherent monolayer in DMEM supplemented with 10% FBS, and have been established as a fully release-tested Master Cell Bank at City of Hope.[7,35] These cells were further genetically modified using an adenovirus carrying the rCE gene (obtained from Dr. Philip Potter at St. Jude Children's Research Hospital).[36,37] Adenoviral transduction was performed with a secretable version of the rCE enzyme (Ad.rCE), as previously described.[12,13]

FE-Pro labeling of NSCs—HB1.F3.CD cells were labeled with FE-Pro as previously described.[16,27] Briefly, Ferumoxide (FE) (Feridex IV, Berlex Laboratories, Wayne, NJ) with a total iron content of 11.2 mg/ml was combined with protamine sulfate (Pro, 1 mg/ml) stock solution (American Pharmaceutical Partners, Schaumburg, IL), added to HB1.F3.CD cells in serum-free DMEM (FE, 100 μg/ml; Pro, 3 μg/ml final concentration) and incubated for 2 h (6% CO_2, 37°C). After 2 h, an equal volume of DMEM plus 10% FBS containing Ad.rCE (MOI = 20) was added to the cells and cells were further incubated for 24 h. After 24 h, cells were washed in PBS containing 10 U/ml of heparin to remove the excess FE-Pro and were used for i.c. or i.v. injections into tumor-bearing mice.

Carboxylesterase enzyme activity assay—Media were derived from HB1.F3.CD.rCE cells (96 h culture) and rCE enzyme activity was measured by conversion of o-nitrophenyl acetate substrate to o-nitrophenol, as determined by spectrophotometry.[25]

NSC migration assay—*In vitro* cell migration assays were conducted using 24-well cell culture plates with polycarbonate inserts (Millipore, Billerica, MA) with pore diameters of 8 μm. Briefly, conditioned media derived from medulloblastoma cells were prepared by addition of serum-free media to cultured cells (~75% confluence), followed by incubation (37°C, 6% CO_2, 48 h). Conditioned media were collected and added to the lower chamber of 24-well plates (600 μl). Inserts were placed into wells, and a suspension of HB1.F3.CD cells was added in the upper chamber (1×10^5 cells per 400 μl) in DMEM supplemented with 2% bovine serum albumin (BSA). After incubation (4 h, 37°C), cells that did not migrate were removed from the upper surface of the filter, whereas migrated cells were detached from the lower surface of the insert by trypsinization. Detached cells were centrifuged at 1500 rpm for 5 min and counted using the Guava ViaCount assay (Guava Technologies, Hayward, CA). Migration assay controls were as follows: negative control, NSCs resuspended in 2% BSA were added to the upper chamber, with 2% BSA in the bottom chamber; positive control, 10% FBS was added to the lower chamber as a chemoattractant.

Cytotoxicity assays—Cells derived from medulloblastoma cells were used for cytotoxicity assays. Human and murine medulloblastoma cells were placed into 96-well plates (3000 cells/well, in triplicate) with final CPT-11 concentrations of 0, 0.1, 1, 10, or 100 μg/ml, or SN-38 concentrations of 0, 0.1, 1, 10, or 100 ng/ml. After incubation for 72 h, viable and dead cells were counted using the Guava ViaCount assay; only viable cells were included in data analysis.

LC-MS/MS assay for CPT-11 and SN-38—LC/MS/MS analysis was performed using a Waters Acquity UPLC system (Milford, MA, USA) interfaced with a Waters Quattro

Premier XE Mass Spectrometer. HPLC separation was achieved using a Synergi Hydro-RP 4μ 150×2.0 mm analytical column (Phenomenex, Torrance, CA, USA) proceeded by a Phenomenex C_{18} guard column (Torrance, CA, USA). The column temperature was maintained at 30 °C, and the flow rate was 0.4 ml/min. The mobile phase consisted of A (20 mM ammonium acetate buffer, pH 3.5) and B (acetonitrile). The following gradient program was used: 20% B (0-3 min), 68% B (6 min), 68% B (6.2 min), 20% B (6.3 min), 20% B (8 min). The total run time was 8 min. The auto-injector temperature was maintained at 5 °C. The electrospray ionization source of the mass spectrometer was operated in positive ion mode with a cone gas flow of 80 L/h and a desolvation gas flow of 700 L/h. The capillary voltage was set to 0.6 kV, and the cone and collision cell voltages were optimized to 60 V and 36 eV for CPT-11, 48 V and 26 eV for SN-38 and 45 V and 23 eV for camptothecin (CPT; internal standard), respectively. The source temperature was 125 °C and the desolvation temperature was 450 °C. A solvent delay program was used from 0 to 4.7 min and from 6.1 to 8 min to minimize the mobile phase flow to the source. MassLynx version 4.1 software was used for data acquisition and processing. Positive electrospray ionization of CPT-11, SN-38, and CPT produced abundant protonated molecular ions (MH+) at m/z 587.31, 393.21 and 349.15, respectively. Fragmentation of these compounds was induced under collision induced dissociation conditions and acidic mobile phase. The precursor→product ion combinations at m/z 587.31→124.14 for CPT-11, 393.21→349.20 for SN-38 and 349.15→305.11 for CPT were used in multiple reaction monitoring mode for quantitation. Under optimized assay conditions, the retention times for CPT-11, SN-38 and CPT were 5.25, 5.43 and 5.62 min, respectively.

Animal models

To initiate an orthotopic xenograft model of human medulloblastoma, 4-week-old *nude/nude* mice received a stereotactic injection of Daoy medulloblastoma cells into the cerebellum (1.0 mm lateral and 1.0 mm posterior from lambda, and 3.0 mm deep from the surface of the skull). NSCs were injected ipsilaterally to the tumor into the cerebellum of mice (1.5 mm lateral, 1.5 mm posterior from lambda, and 3.0 mm deep from the surface of the skull). Migration of the iron-labeled NSCs was monitored by MRI at 1, 4, and 6 days after NSC injection. A transgenic mouse model of medulloblastoma was generated in mice that express the Tva avian retrovirus receptor in the cerebellar granule neuron precursor cells, as well as an eGFP-luciferase fusion protein. Medulloblastomas were produced by intracerebellar injections at postnatal day one to three of nontumorigenic chicken DF-1 cells that produced two avian RCAS retroviral vectors encoding Shh-N, a pre-processed Shh, and a stabilized Mycn mutant (T58A, S62A) (Shackleford et al., manuscript in preparation). The transgenic mice were crosses of the C57BL/6 and DBA/2 strains. Transgenic experiments and tumor cell line isolations were performed with Children's Hospital Los Angeles (IACUC Protocol 190-09). For both models, mice were monitored by MRI every 2 weeks for tumor development. Medulloblastoma-bearing mice received iron-labeled therapeutic NSCs i.v. into the retro-orbital sinus (10^6 cells/100 μl PBS) or i.c. (10^5 cells/2 μl PBS). NSCs were injected into the cerebellum of transgenic mice bearing tumors laterally to Bregma 2.0 mm, 6.7 mm posterior, and 2.5 mm deep from the surface of the skull in order to target region of the multiple medulloblastoma foci (2.0 mm lateral, 6.7 mm posterior from bregma, and 2.5 mm deep from the surface of the skull). All animals were MR imaged at days 1, 4 and 6

after NSC injection to track the distribution of NSCs in the brain. Brain tissue was harvested at day 6 post-NSC administration, and histologic sections were processed for Prussian blue staining to visualize iron-labeled HB1.F3.CD.rCE NSCs. NSC-mediated therapy was evaluated in the transgenic mouse model using the following regimens: 1) HB1.F3.CD.rCE i.c.+ CPT-11 at 20 mg/kg/day i.v. for 4 days; and 2) HB1.F3.CD.rCE i.c. + CPT-11 at 38 mg/kg/day i.v. one dose. The administration of CPT-11 in both regimens was started 4 days after NSC injections. Control mice received CPT-11 only at the same doses as above, and did not receive NSC injections. All therapeutic regimens were repeated once 2 weeks after the start of the first round of treatments (the second NSC injection was into the opposite hemisphere of the cerebellum). Tumor size was monitored by MRI. Mice were euthanized 2 weeks after the start of the second cycle of therapy (total duration of therapy was 30 days). Tissues (brain, liver, spleen, kidneys, bone marrow, lungs, pancreas) were collected and used for immunohistochemistry and Prussian blue staining of iron-labeled NSCs.

3D reconstruction of histological sections

Automatic Cellular Imaging System (ACIS from ChromaVision Medical Systems, Inc., San Juan Capistrano, CA) was used to generate high-resolution images of histological sections (10 μm thick). Three-dimensional reconstruction was performed using Reconstruct (Version 1.1.0.1) software (http://synapses.bu.edu/tools/download.htm). For each tumor, 10 serial brain sections separated by 200 μm imported into Reconstruct and aligned manually. To produce a 3D image, structures of interest were segmented based on color (Prussian blue-label for NSCs) and cell density (tumor areas), and volumes containing these structures were generated using Reconstruct.

Magnetic Resonance Imaging

Anesthesia was induced and maintained with Isofluorane throughout the imaging procedure. Mice were inserted in the prone position into a small animal MRI scanner (PharmaScan 300, Bruker BioSpin Division, Billerica, MA) 7T magnet using the 19 mm inner diameter transmit receive coil. ParaVision 4.0 scanner software was set to use Rapid Acquisition with Relaxation Enhancement (RARE) spin echo sequence for fast T2 weighted imaging (TE 50, TR 3000, RARE Factor 8) with a 256×256 in-plane matrix and 2.56 cm field of view. After scanning, if needed, mice were gently warmed on a thermostatically controlled heating pad until awake enough to be returned to their home cage. MRI images were reconstructed at native resolution. For each mouse, we acquired 22 axial images with 0.4 mm thick slices and 0.02 mm gap between slices. This produced 0.1 mm × 0.1 mm per pixel in-plane resolution with an effective slice thickness of 0.42mm. eFilm Workstation 1.8.1 (eFilm Medical Inc, Toronto, Canada) was used to transfer reconstructed images from DICOM files into TIFF files for further analysis. MetaMorph 6.3 (Molecular Devices, Sunnyvale, CA) was used to open the TIFF files, outline the tumors, count the number of pixels inside each tumor slice, and catalog the data. The number of pixels per slice was converted into tumor volume per slice (tumor volume = pixel count × 0.1 mm × 0.1 mm × 0.42 mm). Tumor volume per slice measurements were summed to produce the final tumor volume per animal.

Statistical analysis

The tumor volume analysis included 14 mice. There were two treatment groups (four mice/group) and two control groups (three mice/group). Measurements were made on each mouse at day 0, day 8 and day 21 after the start of treatment. Two mice died before day 8 (one in control group C2, one in treatment group T2) and these data were not included in the analysis. Three additional mice died before day 21. Day 21 measurements were imputed for these mice using linear regression analysis of the individual mouse's data. This avoids the bias that mice with generally larger tumors died, leaving only the mice with small tumors by day 21.

The analysis was performed for experimental groups as described above using linear mixed effects models implementing the R package nlme.[38-40] The starting model included treatment, days, centered baseline (baseline-mean of the baseline values) and the associated two-way interactions. Tumor growth rate (days) was defined to be random, that is varied with each mouse. Non-significant fixed effects were removed based on p values from t-tests on restricted maximum likelihood (REML) estimates. The final fixed effects portion of the model included center baseline, interaction between days and treatment and associated main effects. The question of interest was: Did the tumor volume growth rates differ between specific treatment and control groups? Comparisons were defined using contrasts and tested with t-tests based on REML estimates. We repeated the analysis, calculating the tumor growth rates for each mouse using simple linear regression, and the results of the predefined contrasts were similar to those of the mixed effects models analysis. The level of significance was set at $p < 0.05$.

Supplementary Material

Refer to Web version on PubMed Central for supplementary material.

Acknowledgments

References

1. Ellison DW. Childhood medulloblastoma: novel approaches to the classification of a heterogeneous disease. Acta Neuropathol. 120:305–316. [PubMed: 20652577]

2. Dubuc AM, Northcott PA, Mack S, Witt H, Pfister S, Taylor MD. The genetics of pediatric brain tumors. Curr Neurol Neurosci Rep. 10:215–223. [PubMed: 20425037]

3. Hatten ME, Roussel MF. Development and cancer of the cerebellum. Trends Neurosci.

4. Ginstfeldt T, Emanuelson I. An overview of attention deficits after paediatric traumatic brain injury. Brain Inj. 24:1123–1134. [PubMed: 20715886]

5. Roussel MF, Hatten ME. Cerebellum development and medulloblastoma. Curr Top Dev Biol. 94:235–282. [PubMed: 21295689]

6. Aboody KS, Najbauer J, Danks MK. Stem and progenitor cell-mediated tumor selective gene therapy. Gene Ther. 2008; 15:739–752. [PubMed: 18369324]

7. Kim SK, Kim SU, Park IH, Bang JH, Aboody KS, Wang KC, et al. Human neural stem cells target experimental intracranial medulloblastoma and deliver a therapeutic gene leading to tumor regression. Clin Cancer Res. 2006; 12:5550–5556. [PubMed: 17000692]

8. Gutova M, Najbauer J, Frank RT, Kendall SE, Gevorgyan A, Metz MZ, et al. Urokinase plasminogen activator and urokinase plasminogen activator receptor mediate human stem cell tropism to malignant solid tumors. Stem Cells. 2008; 26:1406–1413. [PubMed: 18403751]

9. Brown AB, Yang W, Schmidt NO, Carroll R, Leishear KK, Rainov NG, et al. Intravascular delivery of neural stem cell lines to target intracranial and extracranial tumors of neural and non-neural origin. Hum Gene Ther. 2003; 14:1777–1785. [PubMed: 14670128]

10. Pommier Y. Topoisomerase I inhibitors: camptothecins and beyond. Nat Rev Cancer. 2006; 6:789–802. [PubMed: 16990856]

11. Danks MK, Yoon KJ, Bush RA, Remack JS, Wierdl M, Tsurkan L, et al. Tumor-targeted enzyme/prodrug therapy mediates long-term disease-free survival of mice bearing disseminated neuroblastoma. Cancer Res. 2007; 67:22–25. [PubMed: 17210679]

12. Aboody KS, Bush RA, Garcia E, Metz MZ, Najbauer J, Justus KA, et al. Development of a tumor-selective approach to treat metastatic cancer. PLoS One. 2006; 1:e23. [PubMed: 17183650]

13. Arbab AS, Pandit SD, Anderson SA, Yocum GT, Bur M, Frenkel V, et al. Magnetic resonance imaging and confocal microscopy studies of magnetically labeled endothelial progenitor cells trafficking to sites of tumor angiogenesis. Stem Cells. 2006; 24:671–678. [PubMed: 16179427]

14. Arbab AS, Janic B, Knight RA, Anderson SA, Pawelczyk E, Rad AM, et al. Detection of migration of locally implanted AC133+ stem cells by cellular magnetic resonance imaging with histological findings. Faseb J. 2008; 22:3234–3246. [PubMed: 18556461]

15. Thu MS, Najbauer J, Kendall SE, Harutyunyan I, Sangalang N, Gutova M, et al. Iron labeling and pre-clinical MRI visualization of therapeutic human neural stem cells in a murine glioma model. PLoS One. 2009; 4:e7218. [PubMed: 19787043]

16. Ranger A, McDonald W, Moore E, Delmaestro R. The invasiveness of five medulloblastoma cell lines in collagen gels. J Neurooncol. 96:181–189. [PubMed: 19847623]

17. Arbab AS, Wilson LB, Ashari P, Jordan EK, Lewis BK, Frank JA. A model of lysosomal metabolism of dextran coated superparamagnetic iron oxide (SPIO) nanoparticles: implications for cellular magnetic resonance imaging. NMR Biomed. 2005; 18:383–389. [PubMed: 16013087]

18. Packer RJ, Vezina G. Management of and prognosis with medulloblastoma: therapy at a crossroads. Archives of neurology. 2008; 65:1419–1424. [PubMed: 19001159]

19. Vassal G, Boland I, Santos A, Bissery MC, Terrier-Lacombe MJ, Morizet J, et al. Potent therapeutic activity of irinotecan (CPT-11) and its schedule dependency in medulloblastoma xenografts in nude mice. Int J Cancer. 1997; 73:156–163. [PubMed: 9334824]

20. Turner CD, Gururangan S, Eastwood J, Bottom K, Watral M, Beason R, et al. Phase II study of irinotecan (CPT-11) in children with high-risk malignant brain tumors: the Duke experience. Neuro Oncol. 2002; 4:102–108. [PubMed: 11916501]

21. Bomgaars LR, Bernstein M, Krailo M, Kadota R, Das S, Chen Z, et al. Phase II trial of irinotecan in children with refractory solid tumors: a Children's Oncology Group Study. J Clin Oncol. 2007; 25:4622–4627. [PubMed: 17925558]

22. Gutova M, Najbauer J, Chen MY, Potter PM, Kim SU, Aboody KS. Therapeutic targeting of melanoma cells using neural stem cells expressing carboxylesterase, a CPT-11 activating enzyme. Curr Stem Cell Res Ther. 5:273–276. [PubMed: 19951251]

23. Aboody K, Capela A, Niazi N, Stern JH, Temple S. Translating stem cell studies to the clinic for CNS repair: current state of the art and the need for a Rosetta Stone. Neuron. 2011; 70:597–613. [PubMed: 21609819]

24. Frank RT, Edmiston M, Kendall SE, Najbauer J, Cheung CW, Kassa T, et al. Neural stem cells as a novel platform for tumor-specific delivery of therapeutic antibodies. PLoS One. 2009; 4:e8314. [PubMed: 20016813]

25. Aboody KS, Najbauer J, Schmidt NO, Yang W, Wu JK, Zhuge Y, et al. Targeting of melanoma brain metastases using engineered neural stem/progenitor cells. Neuro Oncol. 2006; 8:119–126. [PubMed: 16524944]

26. Aboody KS, Brown A, Rainov NG, Bower KA, Liu S, Yang W, et al. Neural stem cells display extensive tropism for pathology in adult brain: evidence from intracranial gliomas. Proc Natl Acad Sci U S A. 2000; 97:12846–12851. [PubMed: 11070094]

27. Zhao D, Najbauer J, Garcia E, Metz MZ, Gutova M, Glackin CA, et al. Neural stem cell tropism to glioma: critical role of tumor hypoxia. Mol Cancer Res. 2008; 6:1819–1829. [PubMed: 19074827]

28. Gibson P, Tong Y, Robinson G, Thompson MC, Currle DS, Eden C, et al. Subtypes of medulloblastoma have distinct developmental origins. Nature. 2010; 468:1095–1099. [PubMed: 21150899]

29. Read TA, Fogarty MP, Markant SL, McLendon RE, Wei Z, Ellison DW, et al. Identification of CD15 as a marker for tumor-propagating cells in a mouse model of medulloblastoma. Cancer cell. 2009; 15:135–147. [PubMed: 19185848]

30. Gilad AA, Walczak P, McMahon MT, Na HB, Lee JH, An K, et al. MR tracking of transplanted cells with "positive contrast" using manganese oxide nanoparticles. Magn Reson Med. 2008; 60:1–7. [PubMed: 18581402]

31. Artemov D, Mori N, Okollie B, Bhujwalla ZM. MR molecular imaging of the Her-2/neu receptor in breast cancer cells using targeted iron oxide nanoparticles. Magn Reson Med. 2003; 49:403–408. [PubMed: 12594741]

32. Wu X, Hu J, Zhou L, Mao Y, Yang B, Gao L, et al. In vivo tracking of superparamagnetic iron oxide nanoparticle-labeled mesenchymal stem cell tropism to malignant gliomas using magnetic resonance imaging. Laboratory investigation. J Neurosurg. 2008; 108:320–329. [PubMed: 18240929]

33. Neuwelt EA, Varallyay CG, Manninger S, Solymosi D, Haluska M, Hunt MA, et al. The potential of ferumoxytol nanoparticle magnetic resonance imaging, perfusion, and angiography in central nervous system malignancy: a pilot study. Neurosurgery. 2007; 60:601–611. discussion 611-602. [PubMed: 17415196]

34. Lim SH, Choi SA, Lee JY, Wang KC, Phi JH, Lee DH, et al. Therapeutic targeting of subdural medulloblastomas using human neural stem cells expressing carboxylesterase. Cancer Gene Ther. 2011

35. Flax JD, Aurora S, Yang C, Simonin C, Wills AM, Billinghurst LL, et al. Engraftable human neural stem cells respond to developmental cues, replace neurons, and express foreign genes. Nat Biotechnol. 1998; 16:1033–1039. [PubMed: 9831031]

36. Potter PM, Wolverton JS, Morton CL, Wierdl M, Danks MK. Cellular localization domains of a rabbit and a human carboxylesterase: influence on irinotecan (CPT-11) metabolism by the rabbit enzyme. Cancer Res. 1998; 58:3627–3632. [PubMed: 9721871]

37. Wierdl M, Morton CL, Weeks JK, Danks MK, Harris LC, Potter PM. Sensitization of human tumor cells to CPT-11 via adenoviral-mediated delivery of a rabbit liver carboxylesterase. Cancer Res. 2001; 61:5078–5082. [PubMed: 11431344]

38. Orsulic S. An RCAS-TVA-based approach to designer mouse models. Mamm Genome. 2002; 13:543–547. [PubMed: 12420130]

39. Team RDC. R language and Environment for Statistical Computing. R Foundation for Statistical Computing; Vienna, Austria: 2011. www.R-project.org

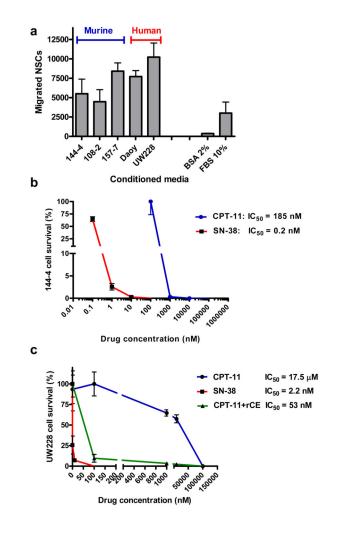40. Pinheiro, JC.; Bates, DM. Mixed effects models in S and S-plus. Springer; New York: 2000.

Figure 1.
(**a**) *In vitro* migration of HB1.F3.CD NSCs to conditioned media derived from mouse cell lines (144-4, 108-2, 157-7) and human medulloblastoma cells (Daoy, UW228) (10% FBS, positive control; 2% BSA, negative control). Dose response of mouse (**b**) and human medulloblastoma (**c**) cells to CPT-11 and SN-38 *in vitro*. Medulloblastoma cells were cultured for 72 h in the presence of the indicated concentrations of CPT-11 or SN-38. Cell survival was normalized to untreated controls. X-axis is $\log_{10}$ scale. Error bars represent standard deviation of quadruplicate measurements.
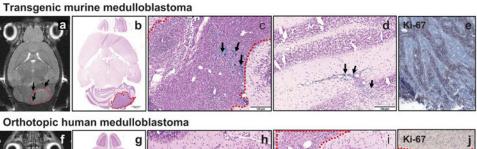
Figure 2.
Experimental mouse models of medulloblastoma. (**a**) Transgenic mouse medulloblastoma 6 weeks after intracerebellar injection of retroviruses carrying Shh and Mycn (H & E). Right panel is enlarged image of boxed area in left panel. (**b**) Orthotopic human medulloblastoma (Daoy) xenograft 5 weeks after intracerebellar injection into *nu/nu* mice (H & E). Right panel is enlarged image of boxed area in left panel. Dashed red lines outline the tumor. Scale bars: 1500 μm (**a**, **b** left panels), 150 μm (**a**, **b** right panels).
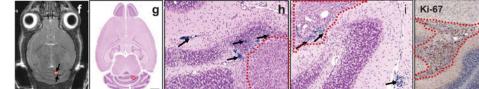
Figure 3.
Visualization of NSCs after intracerebellar administration into tumor-bearing mice. T2-weighted MRI images of transgenic mouse (**a**) and orthotopic human (**f**) medulloblastoma 4 days after intracerebellar injection of iron-labeled HB1.F3.CD NSCs. Tumor (hyperintense signal, dashed red lines) and NSCs (hypointense signal, black arrows). Low- (**b**, **g**) and high-power images (**c**, **d**, **h**, **i**) of sections stained with Prussian blue to identify NSCs (black arrows) and counterstained with pararosaniline (pink). Tumors are outlined by dashed red lines. Ki-67 immunohistochemistry of mouse (**e**) and human (**j**) medulloblastoma in mice. Scale bars: 1500 μm (**b**, **g**), 150 μm (**c**, **d**, **h**, **i**).
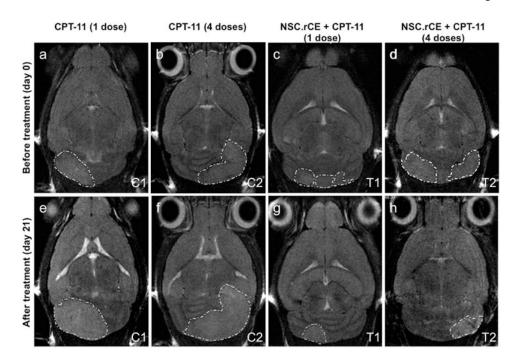
Figure 4.
Evaluation of therapeutic efficacy of NSC.rCE cells plus CPT-11 enzyme/prodrug treatment. MRI images of transgenic mouse medulloblastoma before treatment (day 0) (**a**, **b**, **c**, **d**), and after treatment (day 21) (**e**, **f**, **g**, **h**). Representative axial MRI images of mouse brains from control groups C1 (**a**, **e**) (CPT-11 only, 1 dose 37.5 mg/kg) and C2 (**b**, **f**) (CPT-11 only, 4 doses of 20 mg/kg each), and treatment groups T1 (**c**, **g**) (NSC.rCE + CPT-11, 1 dose, 37.5 mg/kg) and T2 (**d**, **h**) (NSC.rCE + CPT-11, 4 doses of 20 mg/kg each). The therapeutic regimens for these mice were repeated one more time after 2 weeks.
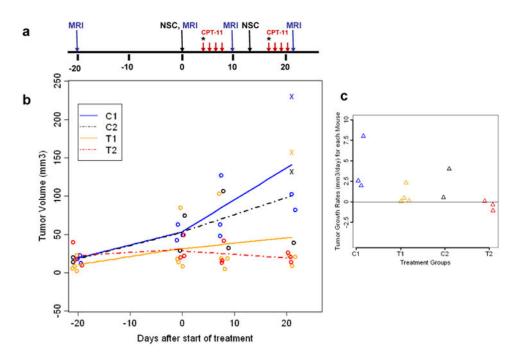
Figure 5.
Statistical analysis: (a) Treatment schema for NSC-mediated CE enzyme/prodrug strategy for transgenic mouse medulloblastoma. Treatment regimens were as described in Figure 4. * Indicates a single dose of CPT-11 injection (37.5 mg/kg), red arrows indicate 4 doses of 20 mg/kg each. (**b**) Graph of the mean tumor growth rates and actual data points before and after treatment for each of the four study groups (C1, C2, T1, and T2). (**c**) Graph of the tumor growth rates after treatment by study group, calculated using linear regression of data for each mouse. Tumor volumes were evaluated using MRI data for each treatment (T1, T2) and control group (C1, C2).